DOI: 10.1063/1.4965231

Quasi-symmetry and the nature of turbulent transport in quasi-poloidal stellarators

J.A. Alcusón, J.M. Reynolds-Barredo, A. Bustos, R. Sanchez and V. Tribaldos
Departamento de Física, Universidad Carlos III de Madrid, 28911 Leganés, Madrid, Spain

P. Xanthopoulos
Max Planck Instutute for Plasma Physics, 17491 Greifswald, Germany

T. Goerler
Max Planck Instutute for Plasma Physics, 85748 Garching, Germany

D.E. Newman
Department of Physics, University of Alaska, Fairbanks, AK 99795, USA
(Dated: April 8, 2016)

It is well known that quasi-symmetric configurations have a better neoclassical confinement compared to that of standard stellarators. It has also been suggested that quasi-symmetries should also result in a better confinement in regards to the radial turbulent transport. In particular, the expected reduction of the neoclassical viscosity along the direction of quasi-symmetry should facilitate the self-generation of zonal flows and, consequently, the suppression of turbulent fluctuations and the ensuing transport. In this paper we show that, at least for quasi-poloidal configurations, the influence of quasi-symmetry on transport exceeds the mere reduction of the fluctuation levels, and that the intimate nature of transport itself is affected. Radial turbulent transport becomes increasingly subdiffusive as the degree of quasi-symmetry becomes larger, whilst transport within the magnetic surface becomes increasingly superdiffusive.

PACS numbers: 52.25.Fi, 52.35.Ra, 52.25.Gj, 05.40.-a

I. INTRODUCTION

An effective manner to confine neoclassical guiding centre orbits is by endowing the confining magnetic field with a hidden symmetry (usually referred to as *quasi-symmetry*), even if just approximately[1,2]. This is best achieved by expressing first the field in Boozer coordinates[3] (s, θ_B, ϕ_B), so that the guiding center motion depends solely on the field magnitude, $B = |\mathbf{B}|$, and its derivatives[4]. Then, the configuration is designed so that the harmonic content of B is dominated by some linear combination, $M\theta_B - N\phi_B$, over as much of the radius as possible. *Quasi-poloidal symmetry* requires that $M = 0$. *Quasi-axisymmetry* (or *quasi-toroidicity)*, that $N = 0$, bringing the configuration closer to a tokamak. Finally, *quasi-helical symmetry*, assumes that $M/N = m_h/n_h$, for some prescribed pair of integers. Examples are provided, respectively, by the QPS[5] (quasi-poloidal) and NCSX[6] (quasi-axisymmetric) projects, that were regretfully cancelled before construction could be started, and by the HSX quasi-helical ($m_h = 1, n_h = 4$) stellarator currently at operation at the University of Wisconsin[7]. Experimental results from HSX have already provided evidence that confirms the improved neoclassical confinement associated to quasi-helical symmetry[8] and the reduced neoclassical viscosity along the quasi-symmetry direction[9]. However, the low-β of HSX plasmas makes it very difficult to characterize if quasi-symmetry has any impact on the radial turbulent transport. It is however expected that, thanks to the reduced neoclassical viscosities, zonal flows able to suppress turbulent fluctuations might be self-generated more easily in these conditions[10]. The available numerical evidence suggests that this seems to be the case, as found for some recent gyrokinetic simulations of electrostatic ITG turbulence in HSX[11] and NCSX[12] numerical equilibria, carried out in computational domains restricted to the neighborhood of a single magnetic surface, for which reduced ion turbulent conductivities have been reported.

In principle, one would expect that turbulence in quasi-poloidal symmetric configurations should be more sensitive to these effects since strong radially-sheared poloidal zonal flows affect radial fluxes the most in configurations with large safety factor. The investigation of whether this is the case is one of the objectives of this paper. However, our study extends beyond the quantification of the level of reduction of the effective ion conductivity due to quasi-poloidal symmetry. Our main objective is to find out whether quasi-symmetries do also alter the intimate nature of radial transport itself, beyond reduced effective transport coefficients. This question is inspired by recent studies reporting a change in the nature of radial turbulent transport across strong, radially-sheared zonal flows in tokamaks[13–15]. In these works, it was found that radial transport became endowed with strong subdiffusive features as the average radial shear of the poloidal angular flow velocity was increased. At the same time, the statistics of the radial velocity fluctuations became strongly non-Gaussian, exhibiting divergent algebraic tails that pointed to the establishment of non-local correlations. From these findings, it was concluded that a phenomenological description of radial transport in terms of effective

coefficients was probably insufficient to capture the transport dynamics in tokamaks the presence of sufficiently strong sheared-flows, and that other models would have to be looked for in order to maintain good predictive capabilities[16–20].

The present paper follows this line of reasoning and investigates whether transport could be similarly affected by the reduction in neoclassical viscosities associated to a larger degree of local quasi-symmetry of a magnetic configuration. We explore this question by characterizing the transport properties of a population of tracer particles as they are advected by electrostatic ITG turbulence computed by the GENE/GIST gyrokinetic code[21] in a quasi-symmetric numerical configuration. Instead of a traditional flux-tube geometry, the computational domain here encompasses all toroidal and poloidal angles, but with a radial domain that is restricted to the radial neighborhood of a reference magnetic surface[11,12], that is labeled by the Boozer radial coordinate $s = s_0$ (see Fig. 1). The degree of quasi-poloidal symmetry at the reference surface s_0 is quantified in terms of the *quasi-symmetry ratio*,

$$\sigma_{\rm qp}(s_0) = \frac{\sum_n |B_{0,n}(s_0)|}{\sum_{m=0}^{M}\sum_{n=-N}^{N} |B_{m,n}(s_0)|} \leq 1. \qquad (1)$$

Perfect quasi-poloidal symmetry would naturally require that $\sigma_{qp} = 1$. For real quasipoloidal configurations, however, σ_{qp} is typically a decreasing function of s. We have taken advantage of this fact and restricted the simulations to a single magnetic configuration, carrying out the gyrokinetic simulations in the neighbourhood of different radial locations(see Fig. 2). In this way, we can maintain a relatively modest variation of the harmonic content of the magnetic field, and still explore a wide range of values of the quasi-symmetry ratio.

The paper is then organized as follows. First, in Sec. II, we will describe the configuration used and the simulations carried out for this study. We will also discuss the fundamentals of TRACER, the new code that has been developed to advance the tracer particles as they are advected by the turbulent potential fields GENE provides. Sec. III will then review some theoretical aspects of fractional transport theory that provide the basis of the diagnostics that will be used to characterize the nature of transport. The characterization of the properties of tracer motion for different quasisymmetry ratios is described in Sec. IV. The interpretation of these results will be discussed in Sec. V. Finally, some main conclusions will be presented in Sec. VI.

II. CONFIGURATION UNDER STUDY

The quasi-poloidal equilibrium configuration chosen for this investigation belongs to a set of cases explored during the design phase of the QPS project[5] (see Fig. 1). It is a configuration with two periods (i.e., $N_{\rm fp} = 2$), aspect ratio $A = R_0/a = 2.6$, $\beta = \langle 2\mu_0 p/B^2 \rangle \sim 2.5\%$, toroidal current $I \sim 40$kA and magnetic field on axis, $B_0 \simeq 0.9$T. Regarding the magnetic harmonic content, the case examined includes poloidal modes varying from $m = 0$ up to $m = M$, with $M = 8$. Regarding toroidal

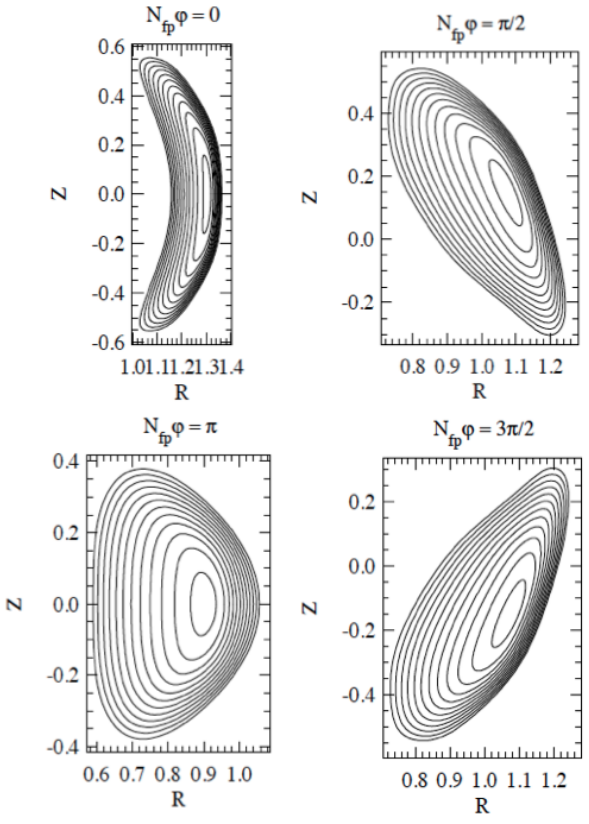

FIG. 1. Cross-sections at four different toroidal angles of the quasi-poloidal configuration used for the GENE simulations discussed in this paper. Number of field periods, $N_{\rm fp} = 2$.

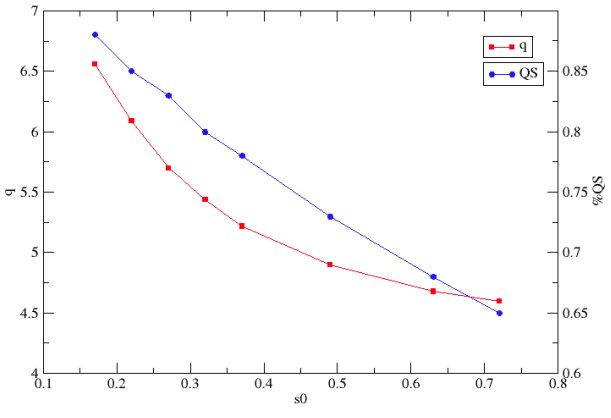

FIG. 2. Safety factor q (red in left axis) and percentage of Quasi-symmetry QS (blue in right axis) for QPS along the radial direction.

modes, they run from $n = -N$ to $n = N$ with $N = 7$. The safety factor decreases smoothly with radius, from $q(0) \simeq 7$ to $q(a) \simeq 4.5$. The quasi-symmetry ratio for this configuration, on the other hand, decreases steadily from slightly below 0.9 close to the axis, to about ~ 0.6 as we reach the edge (see Fig. 2). The poloidal nature of the symmetry can be easily seen when plotting the contour levels of B (see Fig. 1, above frame), that are aligned with the poloidal direction (even when, strictly speaking, the quasi-symmetric alignment is with θ_B, not the geometrical poloidal angle).

We have carried nonlinear gyrokinetic simulations at eight different radial locations for this configuration using the GENE code[21]. These positions have been chosen as to provide a sufficiently wide variation of the quasisymmetry ration (see Fig. 2). At each of them, GENE solves the nonlinear gyrokinetic equations[22] using an Eulerian δf approach with a fixed grid in the 5D phase space $(x, y, z, v_\parallel, \mu)$. It uses a special field-aligned system in which $y = q(s_0)\theta_B - \phi_B$ is constant along a field line, $z = \theta_B$ runs parallel to the magnetic field and $x = \sqrt{s}$ is a normalized radial coordinate. Although originally a flux-tube tokamak code, GENE has been recently extended to be able to deal with fully three-dimensional magnetic configurations[23], such as the one being examined here. In these simulations, the spatial domain considered is an annulus, centered at the reference surface s_0 with $x \in [\sqrt{s_0} - L_x, \sqrt{s_0} + L_x]$. Equilibrium quantities (i.e., gradients, safety factor, etc) are however assumed to be independent of x, keeping their value at s_0 across the whole domain. Periodic boundary conditions in x are also enforced for all perturbed fields. The dominant instability in all simulations is the electrostatic ITG mode (in particular, $a/L_{T_i} = 4$ and $a/L_n = 0$ were used), and assumed adiabatic electrons. The resolution in all cases was set to $126 \times 64 \times 256 \times 32 \times 8$ points in GENE's $(x, y, z, v_\parallel, \mu)$ phase space. These numbers were chosen after having completed systematic linear and nonlinear convergence studies, in which we monitored the saturation levels of various physical variables such as ion heat flux, parallel and perpendicular temperatures, among others. The radial size of the computational domain, for the parameter values used, contains roughly $a/\rho_s \simeq 250$. Finally, the length of all simulations was of the order of several hundreds of Lagrangian turbulent decorrelation times. This was done to ensure that the tracer analysisis could be carried deep into the nonlinear saturated phase, so that long-term transport features could be studied meaningfully.

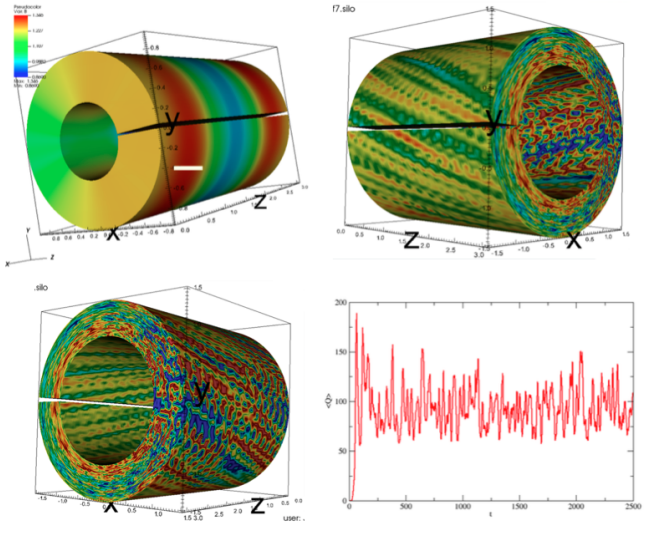

FIG. 3. GENE simulation carried out for the radial position s=0.49 of the quasi-poloidal configuration discussed in the text. All three-dimensional plots are shown in the field-aligned (x, y, z) coordinate system. **Left, above:** $|B|$ showing the (approximated) quasi-poloidal symmetry; **Right, above:** instantaneous potential fluctuations; **Left, below:** instantaneous heat flux; **Right, below:** time evolution of heat flux; black arrows signal the times at which tracer seeding is done.

The techniques that have been used to characterize the nature of transport, and that will be described in Sec. III, require that the trajectories of individual tracers be monitored as they are advected by the electrostatic turbulence calculated by GENE. Advecting particles within modern Vlasov gyrokinetic codes is not trivial due to their large computational cost and their sophisticated but fragile parallel optimization[24]. As a result, the most straightforward way to carry out this type of studies –namely, to include the tracer evolution within the normal Vlasov-Poisson time-stepping– is not very practical. Indeed, it would require a major overhaul of the GK code, specially in order to maintain its internal balance for optimal parallelization and performance. In addition, every time that a different tracer initialization is needed, the whole GK simulation would have to be rerun, thus incurring in a huge waste of computational resources.

For all these reasons, we have developed TRACER, a new parallel code that can carry out, as a post-processing, the advection of as many tracer particles as needed. TRACER obtaines from GENE's standard output all the relevant information that is needed to complete this task including, but not restricted to, the metric tensor and the jacobian (i.e., geometry), the (time-varying) electrostatic potential, the magnetic field and its gradients. TRACER interpolates all these fields in space and in time. The trajectory of each tracer particle, as it is advected by the turbulent $\mathbf{E} \times \mathbf{B}$ drift, is calculated by integrating its equation of motion,

$$\dot{\mathbf{r}} = \mathbf{v}_{\mathrm{E}\times\mathrm{B}} = -\frac{\nabla\phi \times \mathbf{B}}{|\mathbf{B}|^2}, \tag{2}$$

in GENE (x, y, z) own coordinates, using an explicit 4-th order Runge-Kutta (RK4) scheme. Here, ϕ is the turbulent electrostatic potential provided by GENE. Parallel motion and other drifts, although included in TRACER, are not considered in this first study in order to focus on the effects of quasi-symmetry for cross-field turbulence-

induced transport. The initial distribution of tracer particles throughout the computational box can be set at will by the user. Since the annular, local setup of the GENE/GIST runs yields relatively homogeneous turbulence, we have initialized our tracers so that they are uniformly distributed throughout the domain. This initialization is particularly convenient for the Lagrangian diagnostic technique[16,20] that will be used in this work, and that is described in the next section. Its advantage is that it only requires following a few tens of tracer particles ($\sim 10 - 10^2$) over very long periods of time. Many other intializations are however also possible. For instance, tracers could also be positioned at $x = y = 0$ at the start, randomly distributed along the z direction. This setup is more convenient in order to estimate propagators, that have also been used often to characterize the nature of transport[16,19]. However, a much larger number of tracer particles ($\sim 10^5 - 10^6$) is often required in that case to get sufficiently good statistics, since the relevant information is retrieved from the tails of these propagators, that have a much smaller probability.

III. DIAGNOSTICS FOR FRACTIONAL TRANSPORT

The main diagnostic we use in this work to characterize the nature of transport along any particular direction will be the analysis of the statistical and correlation properties of the projection of Lagrangian velocity on that direction. This Lagrangian analysis is one of several constrasted techniques that can be used to characterize the nature of transport in turbulent systems[16,20]. It can be applied very easily to numerical simulations by following in time the evolution of a reduced population of tracer particles as they are advected by the background turbulence.

The technique is based on comparing the properties of the tracer motion with those of fractional Lévy motion (fLm), that we discuss in this section. fLm is a very interesting stochastic model that generalizes the popular Langevin equation from which classical diffusion is often derived. As will be remembered, the Langevin equation for the position of a single particle is given by:

$$x(t) = x_0 + \int_0^t \xi_2(t')dt' \tag{3}$$

where $\xi_2(t)$ is a Gaussian, uncorrelated noise with a correlation function given by $< \xi_2(t)\xi_2(t') >= D\delta(t-t')$. The connection with diffusion is established, for example, by computing the propagator of Eq. 3. Or, in simpler words, the probability of finding the particle at any position x at time $t > 0$. It is given by,

$$P^{\rm LE}(x,t|x_0) = \frac{1}{\sqrt{2\pi Dt}} \exp\left(-\frac{(x-x_0)^2}{2Dt}\right) \tag{4}$$

That is, a Gaussian with standard variation growing as $\sigma^{\rm LE} = (Dt)^{1/2}$. The connection is made after realizaing that this is also the propagator of the classical diffusion equation,

$$\frac{\partial n}{\partial t} = D\frac{\partial^2 n}{\partial x^2}. \tag{5}$$

In a real system, the role of the noise is played by the Lagrangian velocity of the particle, that often follows a correlation function of the form,

$$\langle v(t)v(t')\rangle \simeq v_c^2 \exp\left(-\frac{t-t'}{\tau_c}\right). \tag{6}$$

In this case, the long-term, long-distance limit of transport is also well described by classical diffusion with $D \simeq v_c^2\tau_c$. It follows then that diffusion is ultimately related to the existence of finite characteristic scales for the transport process, v_c and τ_c. Clearly, v_c is related to the (square root of the) variance of the Lagrangian velocitiy; τ_c, on the other hand, determines for how long memory (in the velocity) is maintained as the particle advances along its Lagrangian trajectory.

However, there are situations in which finite transport scales may be absent in a system. In these cases, the Langevin equation is not appropriate to model its transport dynamics. A suitable generalization in these cases is provided by the stochastic equation:

$$x(t) = x_0 + \frac{1}{\Gamma(H-1/\alpha+1)}\int_0^t (t-t')^{H-1/\alpha}\xi_\alpha(t') \tag{7}$$

where $\Gamma(x)$ the Euler's gamma function. The exponent $H \in (0, \max(1, 1/\alpha)]$ is often referred to as the Hurst exponent. On the other hand, $\xi_\alpha(t)$ is an uncorrelated, symmetric Lévy (becoming Gaussian, if $\alpha = 2$) noise with a tail exponent $\alpha \in (0, 2]$, that is no longer a surrogate of the Lagrangian velocity.

Eq. 7 contains several famous stochastic models. For instance, the usual Langevin equation is recovered whenever $\alpha = 2$ and $H = 1/2$. If $\alpha = 2$, but H varies in the range $(0, 1]$, it reduces to the prescription of the famous *fractal Brownian motion* (fBm). In this case, the propagator is still Gaussian but with a standard deviation that grows in time like[25]:

$$\sigma^{\rm fBm} = \frac{(Dt)^H}{(2H)^{1/2}\Gamma\left(H+\frac{1}{2}\right)}. \tag{8}$$

Therefore, the fBm propagator scales diffusively only if $H = 1/2$. Otherwise, transport is termed either *subdiffusive* ($H < 0.5$) or *superdiffusive* ($H > 0.5$). One can study the properties of the Lagrangian velocity of fBm by taking the (proper) derivative of Eq. 7 for $\alpha = 2$. It turns out that[26], although the variance of the Lagrangian velocity (that sets v_c) is well defined, one can no longer define a finite τ_c, since memory is maintained along the Lagrangian trajectory for infinite times if $H \neq 1/2$. As a result, the long-term, long-distance limit of transport is no longer given by classical diffusion.

In the case $\alpha \neq 2$, the propagator takes the form of a symmetric Lévy law[27]:

$$P^{\mathrm{fLm}}(x,t|x_0) = t^{-H} L_{\alpha,\sigma^{\mathrm{fLm}}}\left(\frac{x-x_0}{t^H}\right) \tag{9}$$

with its scale factor σ^{fLm} defined as[27]:

$$\sigma^{\mathrm{fLm}} = \sigma_{\xi_\alpha}\left[(\alpha H)^{1/\alpha}\Gamma\left(H+1-\frac{1}{\alpha}\right)\right]^{-1}, \tag{10}$$

being σ_{ξ_α} the scale factor of the noise Lévy distribution. This type of motion is known as *fractional Levy motion* (fLm)[28]. All moments of the fLm propagator of order α or larger are f however infinite due to the fact that Lévy distributions asymptotically scale as $L_\alpha(x) \propto |x|^{-(1+\alpha)}$ for large values of $|x|$[29]. However, moments of order $p < \alpha$ are still finite, and scale as $\langle (x-x_0)^p \rangle \propto t^{pH}$. By adopting the same fBm conventions, the scaling $H = 1/2$ is still referred to as a diffusive scaling. Consequently, subdiffusion is also used to describe the fLm transport dynamics for $H < 0.5$, superdiffusion, for $H > 0.5$. In the case of fLm, a finite v_c can no longer be defined for the Lagrangian velocity, since their statistics follow a Lévy law with the same tail-index α as the driving noise. In addition, memory is maintained, as in fBm, for infinitely long times along the Lagrangian trajectory for all values of H except for $H = 1/\alpha$.

It is now easy to develop a method to characterize the nature of transport via tracers. One simply needs to determine the exponents α and H that characterize the statistics and the correlation of the component of interest of the tracer Lagrangian velocities, averaged over many tracers[20]. α can be estimated from the tail-index of their statistical distribution. To estimate H, we will use a simple variation of the popular rescaled-range (R/S) method, introduced by Hurst in the 50s to quantify memory in Guassian-distributed time series[30]. Assuming a time series $V_k,\ k = 1, 2, \cdots N$, Hurst's prescription required the computation of the rescaled range:

$$[R/S](\tau) := \frac{\max\limits_{1\leq k\leq \tau} W(k,\tau) - \min\limits_{1\leq k\leq \tau} W(k,\tau)}{\sqrt{\langle V^2\rangle_\tau - \langle V\rangle_\tau^2}}, \tag{11}$$

with

$$W(k,\tau) := \sum_{i=1}^{k} V_i - k\,\langle V\rangle_\tau\,. \tag{12}$$

Here, $\langle\cdot\rangle_\tau$ represents the temporal average up to time τ. When the signal resembles fBm, then $[R/S] \sim \tau^H$, with H being the Hurst exponent. The prescription must however be slightly modified[20] to deal with fLm, due to the divergent nature of its variance. In those cases, the denominator of the rescaled-range is replaced by the $1/s$-th power of a moment of order $s > 0$, with $s < \alpha$.

Therefore, in the next section we will investigate the influence of the degree of quasisymmetry on turbulent transport by estimating the value of α and H averaged over tracer trajectories obtained TRACER using the GK turbulent data provided by GENE at several reference surfaces with varying values of the quasisymmetry ratio. Then, we will monitor whether $\alpha < 2$ and $H \neq 1/2$ to help us track any fundamental change in dynamics that pushes transport away from the standard framework of classical diffusion.

IV. SIMULATION RESULTS

Nonlinear simulations of ITG turbulence have been carried out with GENE/GIST for eight different radial locations within the QPS equilibrium examined (see Fig. 2). The range of quasi-symmetry values explored in this way extends from 0.65, close to the edge, to 0.88 close to the magnetic axis (see Table. I). Hundreds of tracer particles have then been advanced by the TRACER code, over the saturated phase of the turbulence, using the electrostatic potential provided by GENE/GIST. The amount of time that orbits are advanced correspond to several hundreds of Lagrangian decorrelation times, since it is the long-term transport that we are interested in.

A. Radial transport

The first result worth mentioning in regards to radial transport is that, consistently with previous nonlinear simulations realized for other type of quasi-symmetries (i.e., quasi-helical[11] and quasi-axisymmetric[12]), the effective heat conductivity, computed as the average:

$$\chi_{i,\mathrm{eff}} = \left\langle \frac{-q_r^i}{dT_i/dr} \right\rangle_{\mathrm{volume}}, \tag{13}$$

(being $\mathbf{q}^i$ the ion heat flux), becomes smaller as the values of the quasi-symmetry ratio σ_{qp} grow (see Fig. 4). The reduction is positively correlated with the capability of self-generated, radially sheared flows to act on turbulence. We have chosen to characterize this correlation in terms of the figure-of-merit,

$$\omega := \left\langle \left| \frac{d}{dx}\left(\mathbf{v}_{\mathrm{E\times B}} - \frac{\mathbf{v}_{\mathrm{E\times B}}\cdot\nabla x)\nabla x}{g^x x} \right) \right| \right\rangle_{\mathrm{volume}} \tag{14}$$

that roughly estimates the radial variation of the

This reduction is clearly correlated with the expected increase in the , that we have chosen to characterize in terms of the figure-of-merit $\partial_x(v_y/\sqrt{g})$, that roughly estimates the radial derivative of the local (mostly poloidal) angular velocity.

In order to tell whether the change in transport dynamics if more profound than a mere reduction of the effective conductivity, we have also estimated the values of the two transport exponents α and H that characterize the propagator associated to radial motion of the tracer particles. As described in Sec. III, the estimation is done by comparing the numericall obtained tracer propagators

with those of fLm. The method is illustrated, for one of the tracer seedings realized in the nonlinear simulation centered at $s_0 = 0.27$, in Fig. 6. The values obtained from the analysis of all radial locations, after averaging over multiple seeding cycles, have been collected in Table I. The resulting value of the exponent $\beta = \alpha H$, defined in Eq. **??**, is also included.

Clearly, the value of the Hurst exponents obtained lie below 0.5 in all simulations, which means that radial transport of tracers is not diffusive (with a lower diffusivity), but subdiffusive. Furthermore, the value of H consistently decreases as the value of the quasi-symmetry ratio increases. Thus, transport becomes more strongly subdiffusive as we approach the center of the configuration, and becomes less so as we move towards the edge. It is also apparent that there is no location in the chosen quasi-poloidal configuration where the quasi-symmetry ratio becomes sufficiently low so that transport behaves diffusively. This means that the relevant poloidal viscosity nevers becomes so large as to prevent the development of a meaningful zonal flow.

Secondly, we also observe that the radial propagator exhibits a fat power-law tail in all locations. That is, $G(x,t|x_0) \sim |x - x_0|^{-(1+\alpha)}$, with $\alpha \sim 0.75$ close to the center, where the quasi-symmetry ratio is larger, $\sigma_{\rm qp} \sim 0.88$. The value of α then increases consistently, reaching its maximum, $\alpha \sim 1.95$ at the outermost position, that also has the lower quasi-symmetry ratio, $\sigma_{\rm qp} \sim 0.65$.

Finally, we find that the value of the exponent $\beta = \alpha H$, that quantifies the degree of non-Markovianity of the transport dynamics, remains significantlly smaller than 1 everywhere. The lowest value, $\beta \sim 0.24$, happens close to the center, where the value of the quasi-symmetry ratio is larger, and then steadily increases towards one as we approach the edge.

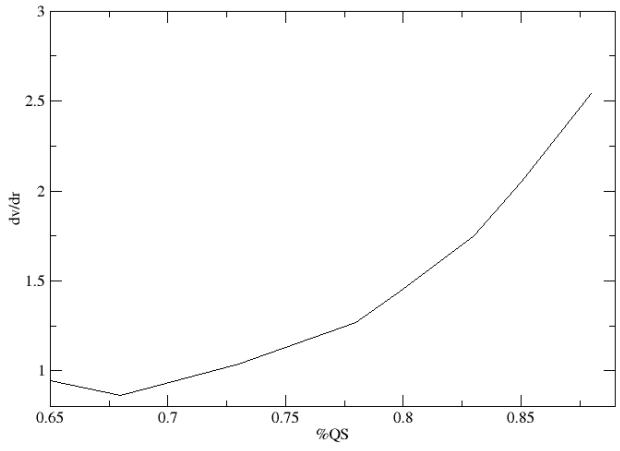

FIG. 4. Sheared flow strength, as measured by the figure-of-merit $\left\langle \left| \frac{d}{dx}\left(\frac{v_\theta}{\sqrt{g}}\right)\right|\right\rangle$, as function of the degree of quasi-symmetry QS. **Jorge: In this same figure, in the opposite axis, we should include the values of the effective ion conductivity χ as a function of the quasi-symmtery ratio.**

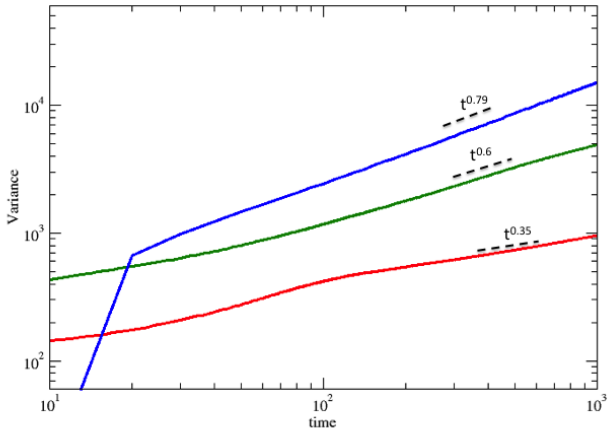

FIG. 5. **Jorge, it would be better to show here a comparison of propagators and tracer densities from the fitting code for three different times, illustrating the idea α. Then, we can show the variance as a function of time for that case, illustrating the subdiffusive H.**

B. Transport along y (i.e., almost poloidal)

We have also estimated the transport exponents that characterize the propagator associated to the tracer motion along the y direction. That is, the direction that is perpendicular both to the magnetic field line and the radial direction, and that approaches the poloidal direction as $q \gg 1$. We have collected in Table II the exponents resulting from the comparison of the numerical propaga-

s_0	$\sigma_{\rm qp}$	$\left\langle \left\| \frac{d}{dx}\left(\frac{v_\theta}{\sqrt{g}}\right)\right\|\right\rangle$	H	α	β
0.17	0.88	2.54	0.33	0.74	0.24
0.22	0.85	2.05	0.35	1.02	0.36
0.27	0.83	1.75	0.40	1.30	0.52
0.32	0.80	1.45	0.43	1.34	0.57
0.37	0.78	1.27	0.44	1.56	0.68
0.49	0.73	1.04	0.44	1.60	0.70
0.63	0.68	0.87	0.44	1.82	0.82
0.72	0.65	0.94	0.45	1.94	0.87

TABLE I. Transport exponents characterizing the radial propagators for the tracer motion along the x (i.e., radial) direction obtained from the eight GENE nonlinear runs carried out, as explained in text.

tors against those of fLm discussed in Sec. III.

In this case, the trend obtained for the Hurst exponent is completely opposite to what we found for the radial motion. Indeed, the transport of tracers along y is clearly superdiffusive for all locations, with values of $H > 0.5$ everywhere. Note, however, that these transport does not correspond to mere free-streaming along y, that would require $H = 1$. We find that the value of H steadily decreases as we move outwards into regions where the value of the quasi-symmetry ratio decreases. For instance, $H \sim 0.9$ at the innermost location, where $\sigma_{\rm qp} = 0.844$, and $H \sim 0.60$ for $\sigma_{\rm qp} = 0.65$, very close to the edge.

Secondly, all the poloidal propagators examined do exhibit fat tails with $\alpha < 2$. Similarly to what we found along the radial direction, the fattest tails are also found here at the locations with larger values of the quasi-symmetry ratio. Thus, $\alpha \sim 0.8$ for $\sigma_{\rm qp} = 0.844$, with the value of α consistently increasing towards the Gaussian one ($\alpha = 2$) as one moves outwards and the quasi-symmtery ratio decreases.

Finally, we proceed to discuss the values obtained for the exponent $\beta = \alpha H$. In contrast to the radial case, we find now that $\beta \sim 1$ is obtained almost everywhere, except perhaps at the inner locations with the highest quasi-symmetry ratio values. This is an interesting observation, that suggest that non-local, and not so much non-Markovian effects, could be more important in setting the nature of the tracer motion along y.

V. DISCUSSION

The results described in the previous section suggest that, although a reduced effective conductivity does indeed follow from an increase in the degree of quasi-poloidal symmetry, this observation is far from providing a complete picture of what is going on. Clearly, the nature of radial transport becomes more subdiffusive as the degree of quasi-symmetry increases and, simultaneously, poloidal transport becomes more superdiffusive. The fact that these trends also seem correlated with an increase

s_0	$\sigma_{\rm qp}$	$\left\langle \left\vert \frac{d}{dx}\left(\frac{v_\theta}{\sqrt{g}}\right)\right\vert \right\rangle$	H	α	β
0.17	0.88	2.54	0.84	0.83	0.70
0.22	0.85	2.05 1	0.81	0.96	0.78
0.27	0.83	1.75	0.79	1.17	0.92
0.32	0.80	1.45	0.76	1.22	0.93
0.37	0.78	1.27	0.69	1.26	0.87
0.49	0.73	1.04	0.66	1.43	0.94
0.63	0.68	0.87	0.59	1.80	1.06
0.72	0.65	0.94	0.60	1.77	1.06

TABLE II. Transport exponents obtained for the motion of tracers along y (almost poloidal) direction. Errors are obtained by averaging over seedings, as explained in text.

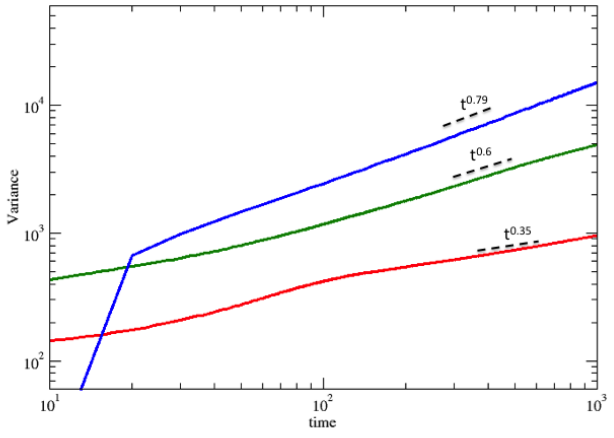

FIG. 6. **Jorge, it would be better to show here a comparison of poloidal propagators and tracer densities from the fitting code for three different times, illustrating the idea α. Then, we can show the variance as a function of time for that case, illustrating the superdiffusive H.**

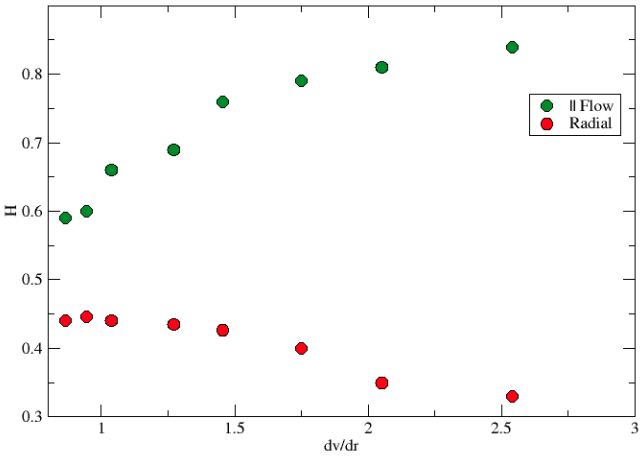

FIG. 7. **Above:** Hurst exponent H for motion along the x (red) and y (green) directions as a function of the flow shearing strength, $\langle \partial_x v_y/\sqrt{g}\rangle_{xyz}$. **Middle:** Tail exponent α for motion along the x (red) and y (green) directions as a function of the flow shearing strength. **Below:** Memory exponent β for motion along the x (red) and y (green) directions as a function of the flow shearing strength .

in the shearing capability of the poloidal zonal flow, as quantified by the figure-of-merit $\langle \partial_x v_y/\sqrt{g}\rangle_{xyz}$, suggests that the action of the sheared flow, that is made easier by the reduced neoclassical viscosity often associated to a higher degree of symmetry, lies at the heart of the explanation for the observed behaviour.

It would appear that the same mechanism that was in-

voked to explain the subdiffusive radial transport found in tokamaks[13,15] might be responsible for the behavior found in the quasi-poloidal nonlinear simulations. If that were indeed the case, it should be expected that a large positive [negative] value of $\langle \partial_x v_y/\sqrt{g}\rangle_{xyz}$ would cause that, in addition to the concomittant streching along y and the shortening along x of any region of localized vorticity (along z) driven by the sheared local poloidal rotation, a reinforcement of those regions with positive vorticity together with a suppresion of those with opposite sign would follow[15]. As a result, it should become more probable that any radial motion would often reverse direction, thus leading to subdiffusion along x. Simultaneously, the same reinforcing process would favour that poloidal motion will continue along its current direction with a larger probability. Thus, superdiffusive transport should follow along y. Fig. 7 shows that this is indeed what is happening in the quasi-poloidal simulations.

Regarding the non-Gaussian tails found in the radial propagators, they can also be understood here along the lines of the same mechanism previously proposed for tokamaks. That is, to the interaction of the fluctuating part of the zonal flow with the local fluctuations, whose dynamics somewhat resemble those of a predator-prey system[15]. The same cannot be said, however, about the power-law tails found in the poloidal propagators, since the avalanching process is intrinsic to radial propagation. A different physical process must probably be at work, that we have not been able to identify yet. One hint towards the nature of this process might be provided by the fact that $\beta \simeq 1$ for poloidal motion *independently of the shearing strength of the poloidal flow*, in contrast to what is observed for radial motion (see lower frame of Fig. 7). This suggests that poloidal motion might be Markovian, in contrast to the radial one, and that all its non-diffusive features appear through the value of α alone, what would perhaps be a reflection of a possible fractal nature of the spatial landscape in which the tracer particles move. The soundness of this speculation will certainly be investigated in the future.

VI. CONCLUSIONS

We have shown that quasi-poloidal symmetry may improve the confinement properties of a magnetic configuration in regards to turbulent transport. However, this enhancement is caused by a profound change in the nature of radial transport, that trascends the mere reduction of transport effective coefficients. Instead, the reduced viscosity associated to the presence of the symmetry allows the development of poloidal flows with a larger shearing strength that modify the vorticity landscape in such a way that subdiffusive transport follows across the direction prependicular to the flow, whilst superdiffusion dominates transport along the flow. The physical mechanisms responsible for these behaviours are very similar to what has been recently observed in tokamaks, at least in the radial direction. Regarding transport along the poloidal direction, the responsible mechanism is not clear. This situation was not studied previously in tokamaks either, so that it leaves an interesting open problem to address in the future.

ACKNOWLEDGMENTS

This research was carried in part at the Institute fur Plasmaphysik of the Max-Planck Institut in Greifswald (Germany), whose hospitality is gratefully acknowledged by some of us (JAA, RS, VT). This research was funded in part by the Spanish National Project No. ENE2012-33219. GENE simulations have been run thanks in part to a continued grant to use the *MareNostrum* supercomputer at BSC (Barcelona, Spain). TRACER runs carried out in the supercomputer cluster *Quadrivium* located at Universidad Carlos III de Madrid (Spain) and ha funded by the Spanish Government via the national projects UNC313-4E-2361, ENE2009-12213-C03-03, ENE2012-33219 and ENE2012-31753.

[1] AH. Boozer. *Rev. Mod. Phys.* **76** 1071?1141 (2004).
[2] P. Helander. *Rep. Prog. Phys.* **77** 087001 (2014).
[3] A.H. Boozer. *Phys. Fluids* **25**, 520 (1982).
[4] R.B. White, A.H. Boozer and R. Hay. *P*hys. Fluids **25**, 575 (1982).
[5] D.A. Spong, S.P. Hirshman, L.A. Berry, J.F. Lyon, R.H. Fowler, D.J. Strickler, M.J. Cole, B.E. Nelson, D.E. Williamson, A.S. Ware, D. Alban, R. Sanchez, G.Y. Fu, D.A. Monticello, W.H. Miner and P.M. Valanju. *Nucl. Fusion* **41**, 711-716 (2001).
[6] M.C. Zarnstorff, L.A. Berry, A. Brooks, E. Fredrickson, G.-Y. Fu, S Hirshman, S. Hudson, L.-P. Ku, E. Lazarus, D. Mikkelsen, D. Monticello, G. H. Neilson, N. Pomphrey, A. Reiman, D. Spong, D. Strickler, A. Boozer, W.A. Cooper, R. Goldston, R. Hatcher, M .Isaev, C. Kessel, J. Lewandowski, J.F. Lyon, P. Merkel, H. Mynick, B. E. Nelson, C. Nuehrenberg, M. Redi, W. Reiersen, P. Rutherford, R. Sanchez, J. Schmidt and R. B. White. *Plasma Phys. Control. Fusion* **43**, A237-A249, (2001).
[7] F. S. B. Anderson, A. F. Almagri, D. T. Anderson, P. G. Mathews, J. N. Talmadge and J. L. Shohet, *Fus. Technology* **27**, 273 (1995).
[8] J.M. Canik, D.T. Anderson, F.S.B. Anderson, K.M. Likin, J.N. Talmadge and K. Zhai. *Phys. Rev. Lett.* **98**, 085002 (2007)
[9] S.P. Gerhardt, J.N. Talmadge, J.M. Canik and D.T. Anderson. *Phys. Rev. Lett.* **94**, 015002 (2005).
[10] P.W. Terry. *Rev. Mod. Phys.* **72**, 109 (2000).
[11] W. Guttenfelder, J. Lore, D.T. Anderson, F.S.B. Anderson, J.M. Canik, W. Dorland, K.M. Likin and J.N. Talmadge. *Phys. Rev. Lett.* **101**, 215002 (2008).

[12] H. E. Mynick, N. Pomphrey and P. Xanthopoulos *Phys. Rev. Lett.* **105**, 095004 (2010).
[13] R. Sanchez, D.E. Newman, J. N. Leboeuf, V.K. Decyk and B.A. Carreras *Phys. Rev. Lett.* **101** 205002 (2008).
[14] R. Sanchez, D.E. Newman, J.N. Leboeuf, B.A. Carreras and V.K. Decyk *Phys. Plasmas* **16** 055905 (2009)
[15] R. Sanchez, D.E. Newman, J.N. Leboeuf and V.K. Decyk *Plasma Phys. Control. Fusion* **53** 074018 (2011).
[16] R. Sanchez and D.E. Newman. *Plasma Phys. Contr. Fus.* **57**, 123002 (2015).
[17] B.A. Carreras, V.E. Lynch and G.M. Zaslavski *Phys. Plasmas* **8** 5096 (2001).
[18] B.Ph. Milligen, R. Sanchez and B.A. Carreras *Phys. Plasmas* **11** 2272 (2004).
[19] D. del-Castillo-Negrete, B.A. Carreras and V.E. Lynch *Phys. Rev. Lett.* **94** 065003 (2005).
[20] J. A. Mier, R. Sanchez, L. Garcia, B.A. Carreras, D.E. Newman *Phys. Rev. Lett.* **101** 165001 (2008).
[21] F. Jenko, W. Dorland, M. Kotschenreuther and B.N. Rogers *Phys. Plasmas* **7**, 1904 (2000).
[22] A.J. Brizard and T.S. Hahm *Rev. Mod. Phys.* **79**, 421 (2007).
[23] P. Xanthopoulos, W.A. Cooper, F. Jenko, Y. Turkin, A. Runov and J. Geiger. *Phys. Plasmas* **16**, 082303 (2009).
[24] T. Hauff and F. Jenko *Phys. Plasmas* **13** 102309 (2006).
[25] B.B. Mandelbrot and J.W. van Ness. *SIAM Review* **10**, 422-437 (1968).
[26] R. Sanchez, B.A. Carreras, D.E. Newman, V. Lynch and B.Ph. van Milligen *Phys. Rev. E* **74** 016305 (2006).
[27] I. Calvo and R. Sanchez, *J. Physics A* **42**, 055003 (2009).
[28] N. Laskin, I. Lambadaris, F.C. Harmantzis and M. Devetsikiotis. *Comp. Networks* **40**, 363-375 (2002).
[29] G. Samorodnitsky and M.S. Taqqu. *Stable non-Gaussian processes*. Chapman and Hall, New York (1994).
[30] H. E. Hurst, *Trans. Am. Soc. Civ. Eng.* **116**, 770 (1951).